Proposal to perform an experiment at the A2 hall, MAMI:
"High Precision Measurement of the ep elastic cross section at small Q^2"

Contact person for the Experiment:
Alexey Vorobyev, Petersburg Nuclear Physics Institute
Mainz contact person: Achim Denig, Institute for Nuclear Physics, JGU Mainz

Abstract

This experiment is motivated by the observed striking difference (4%) in the proton radius values extracted from elastic ep scattering and from muonic Lamb shift experiments ("proton radius puzzle"). The proposed experiment aims for a high resolution high precision measurement of the differential ep elastic cross sections in the region of low momentum transfer: $0.002 \leq Q^2 \leq 0.04$ GeV^2. More than 100 resolved experimental points will be obtained in this region with 0.2% absolute precision in dσ/dt. This will allow extracting the proton radius with 0.6% precision, which could be decisive in solving the "proton radius puzzle".

The experiment will be performed with a low-intensity electron beam at MAMI. An active hydrogen target - specially developed for this experiment - detecting recoil protons will be used in combination with a high precision tracker detecting the scattered electrons. This device allows to measure: the recoil proton energy, the recoil proton angle, and the angle of scattered electron.

MAMI Specifications

Beam energy	500 MeV, 720 MeV
Energy spread	< 20 keV (1σ)
Energy shift	< 20 keV (1σ)
Absolute energy	±< 150 keV (1 σ)

Electron Beam Specifications

Beam intensity (main run)	2x10^6 e/sec
Beam intensity for calibration	10^4 e/sec and 10^3 e/sec
Beam divergency	≤ 0.5 mrad
Beam size	minimal at given divergence

Beam Time Request

Test run in 2017	~ 2 weeks
First physics run in 2018	~ one month

1. Introduction

The striking difference in the proton radius values extracted from the elastic ep scattering experiments (Rp =0.887 (5)) and from the muonic Lamb shift experiments (Rp = 0.88409 (4)) is widely discussed in scientific community [1]. It is generally agreed that new experiments are needed to resolve this puzzle. In particular, new high precision measurements of differential cross sections of the ep elastic scattering in the low Q^2 region are important.

The ep elastic scattering cross sections are given by the following expression:

$$\frac{d\sigma}{dt} = \frac{\pi\alpha^2}{t^2}\left\{G_E^2\left[\frac{\left(4M + t/\varepsilon_e\right)^2}{4M^2 - t} + \frac{t}{\varepsilon_e^2}\right] - \frac{t}{4M^2}G_M^2\left[\frac{\left(4M + t/\varepsilon_e\right)^2}{4M^2 - t} - \frac{t}{\varepsilon_e^2}\right]\right\} \quad (1)$$

where $t = -Q^2$, $\alpha = 1/137$, ε_e - initial electron energy, M – proton mass, G_E – electric form factor and G_M – magnetic form factor.

At low Q^2 the form factors can be represented by the expansions:

$$\frac{G\left(Q^2\right)}{G\left(0\right)} = 1 - \frac{1}{6}\left\langle R_p^2\right\rangle Q^2 + \frac{1}{120}\left\langle R_p^4\right\rangle Q^4 - \ldots, \quad (2)$$

The electric proton radius R_{pE} can be measured by measuring the slope of the electric form factor G_E as Q^2 goes to 0:

$$R_{pE}^2 = \left.\frac{-6 \cdot dG_E\left(Q^2\right)}{dQ^2}\right|_{Q^2 \to 0} \quad (3)$$

The region of $Q^2 \le 0.02$ GeV^2 seems to be optimal for such measurements as the nonlinear effects, essential at higher transfer momenta, should not yet appear at $Q^2 = 0.02$ GeV^2. Also, contribution of magnetic scattering in this region is quite small.

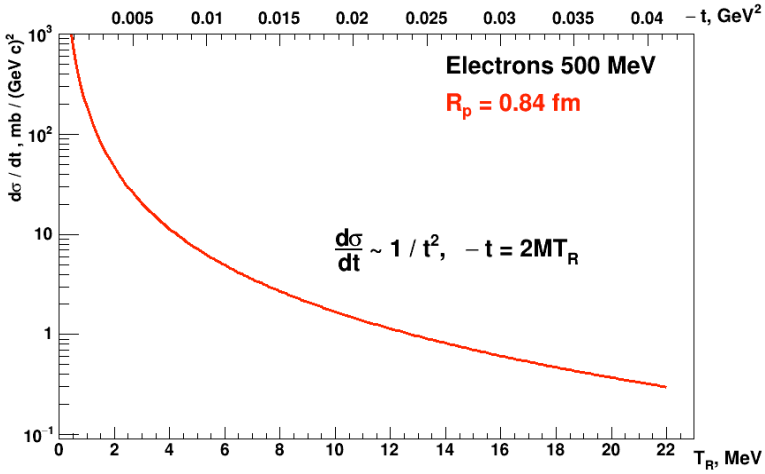

Fig.1. *Differential cross section of ep scattering calculated for ε_e =500 MeV.*

The sensitivity of dσ/dt to the proton radius at $Q^2 \le 0.02$ GeV^2 is rather small, however, as it is demonstrated in Fig 2. This figure shows the ratio of dσ/dt calculated for two different values of Rp to that calculated for a point-like proton. The cross sections corresponding to Rp =0.88 fm and Rp=0.84 fm differ only by 1.3% at $Q^2 = 0.02$ GeV^2 (Fig.3). That means that at least 0.2% precision in measurements of dσ/dt in the region $Q^2 \le 0.02$ GeV^2 is needed to distinguish reliably between these two options. As to the lowest Q^2 required in these measurements, it could be 0.001-0.002 GeV^2 where dependence of dσ/dt on the proton radius becomes small enough (0.7%-1.4%, respectively).

The measurements need high Q^2 resolution to have as many resolved points in the studied Q^2 region as possible – this would be an important control for the $G_E(Q^2)$ linearity.

The measurements of the slope in $G_E(Q^2)$ could be relative that is without absolute normalization of dσ/dt, as it was in all previous measurements, but it is highly desirable to have absolute measurements of dσ/dt. In this case, the measured $(d\sigma/dt)_{expt}$ (after radiative corrections) could be directly compared with the theoretical $(d\sigma/dt)_{theory}$, thus providing control over the calculated radiative corrections and making measurements of the proton radius more reliable.

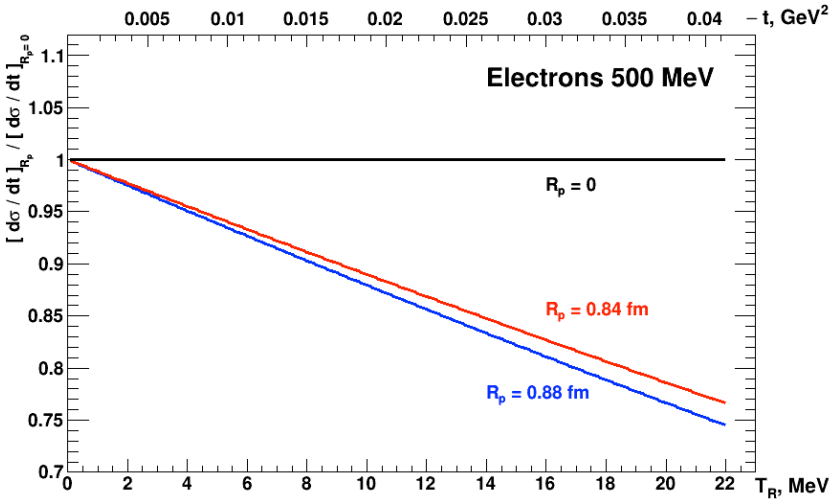

Fig.2. *Ratio of dσ/dt calculated for two different values of Rp to that calculated for a point-like proton.*

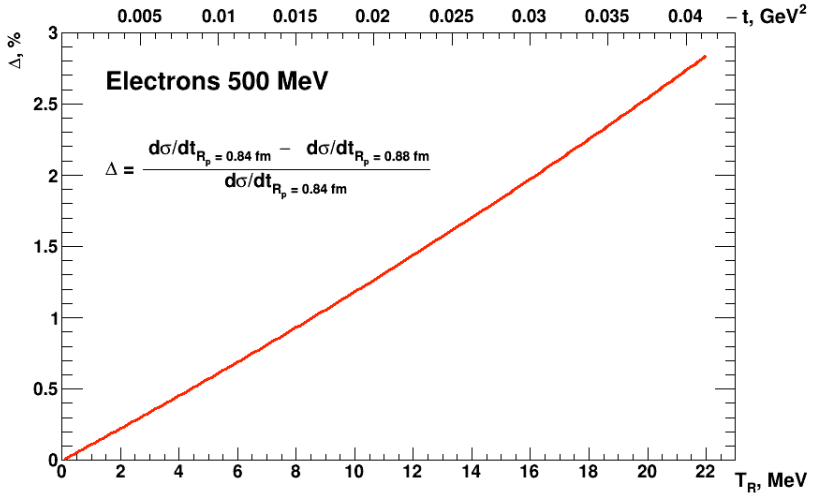

Fig.3. *Difference between the ep differential cross sections corresponding to Rp=0.84 fm and Rp=0.88 fm.*

The requirements to the new generation measurements of the proton radius in ep scattering experiments could be summarized as follows:

* Low transfer momentum region, 10^{-3} GeV$^2 \le Q^2 \le 2\cdot10^{-2}$ GeV^2;
* High resolution in Q^2;
* Absolute measurements of dσ/dt with 0.2% precision.

The first experiment designed to meet such requirements is the PRad experiment at Jefferson laboratory. This experiment studies the electron scattering on the hydrogen gas jet target. The transfer momentum is determined by the electron scattering angle,

the energy of the scattered electron is measured by a calorimeter, the measured ep cross sections are normalized to the simultaneously measured Møller cross sections. The PRad experiment was approved in 2012, and it began data taking in 2016.

The experiment presented in our proposal has similar goals but it is based on a different experimental method. Therefore, these two experiments will be complementary to each other, thus increasing the confidence in the obtained results.

2. Experimental overview

An active hydrogen target - Time Projection Chamber (**TPC**) - detecting recoil protons will be used in combination with a high precision tracker detecting the scattered electrons. Fig.4 shows a schematic view of the proposed experimental setup. It contains hydrogen TPC and a MWPC based Forward Tracker (**FT**).

The TPC operates in the ionization mode (no gas amplification). It allows to measure: the recoil proton energy T_R, the recoil proton angle θ_R, and the z -coordinate of the vertex Z_V. The X_V- and Y_V-coordinates are determined from the beam telescope.

The FT consists of two pairs of Cathode Strip Chambers (**CSC**) X_1/Y_1 and X_2/Y_2 interspaced by 100 mm. The CSCs measure the X_1/Y_1 and X_2/Y_2 coordinates of the scattered electrons. The scattering angle θ_e is determined using the measured $Z_V/X_V/Y_V$ and X_1/Y_1 coordinates (the main mode) or X_1/Y_1 and X_2/Y_2 coordinates (complimentary mode).

Outside the volume of the main detector, beam detectors made of Si-pixels are placed. They determine the beam electron trajectories and provide absolute counting rate of the beam electrons for measurements of the absolute cross sections. In addition, the downstream beam detector includes two scintillator counters. One of them can be used as a beam killer, the other one will detect the pileups of the beam electrons.

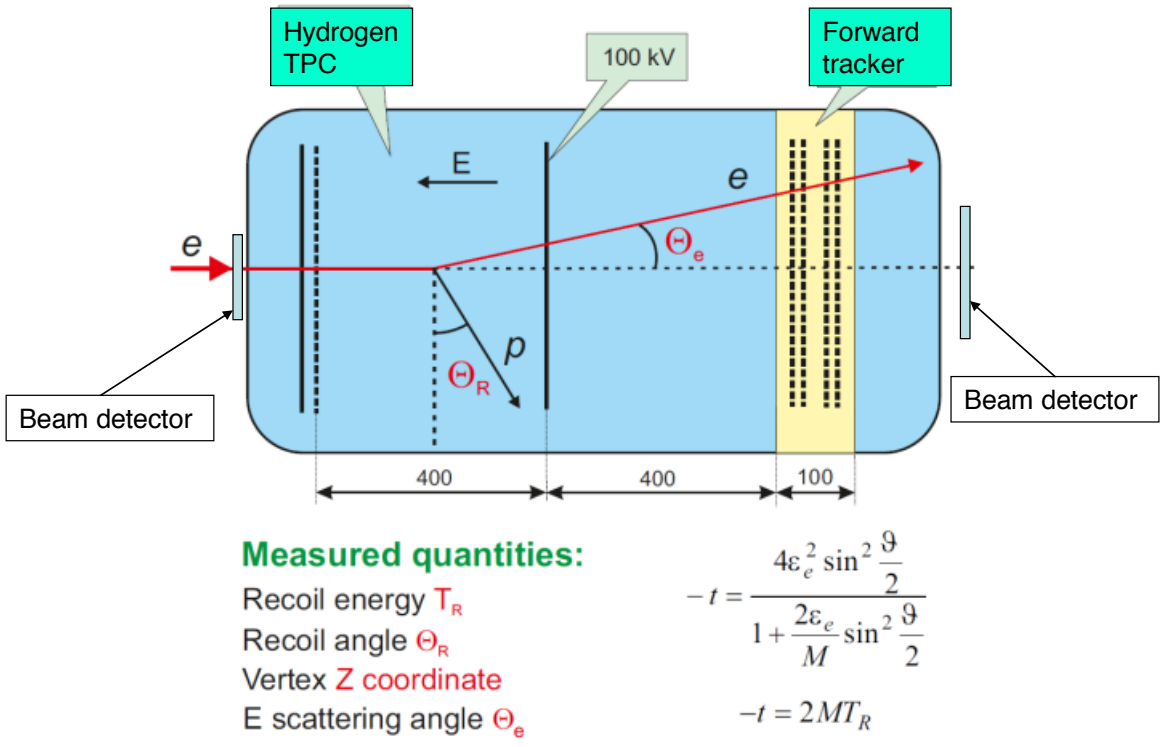

Fig. 4. *Schematic view of the combined TPC & FT detector.*

The transfer momentum, –t, can be determined either by the recoil proton energy T_R or from the scattering angle of the elctron θ_e. The advantage of the T_R method is that it determines the transfer momentum independently of the initial electron energy ε_e:

$$-t = 2MT_R \,. \tag{4}$$

At small transfer momentum, the ep differential cross section is practically independent on the initial electron energy at $\varepsilon_e \geq 500$ MeV. Therefore, measurements of dσ/dt by the T_R method are not sensitive to possible uncertainties in ε_e. This is especially important for ep scattering. Note that already after 0,5 mm Be (which is the thickness of the TPC entrance window) the energy tail contains 2%, 0.9%, 0.7%, 0.3 %, and 0.2% of the beam intensity with the energy losses more than 1 MeV, 5 MeV, 10 MeV, 50 MeV, and 100 MeV, respectively, for 500 MeV electrons (Fig.5). In addition, there will be some more materials: beam detector, hydrogen in TPC. Fortunately, by measuring t-values by the T_R method, we avoid the influence of this tail on the measured dσ/dt.

On the contrary, the t-value determined via the electron scattering angle θ_e depends on ε_e :

$$-t = \frac{4\varepsilon_e^2 \sin^2\frac{\vartheta}{2}}{1+\frac{2\varepsilon_e}{M}\sin^2\frac{\vartheta}{2}} \tag{5}$$

Therefore, the tail in ε_e creates a tail in t-values and disturbs the dσ/dt measurement. On the other hand, the θ_e scale can be prepared with high absolute precision. This allows using the θ_e - T_R correlation for precise T_R scale calibration.

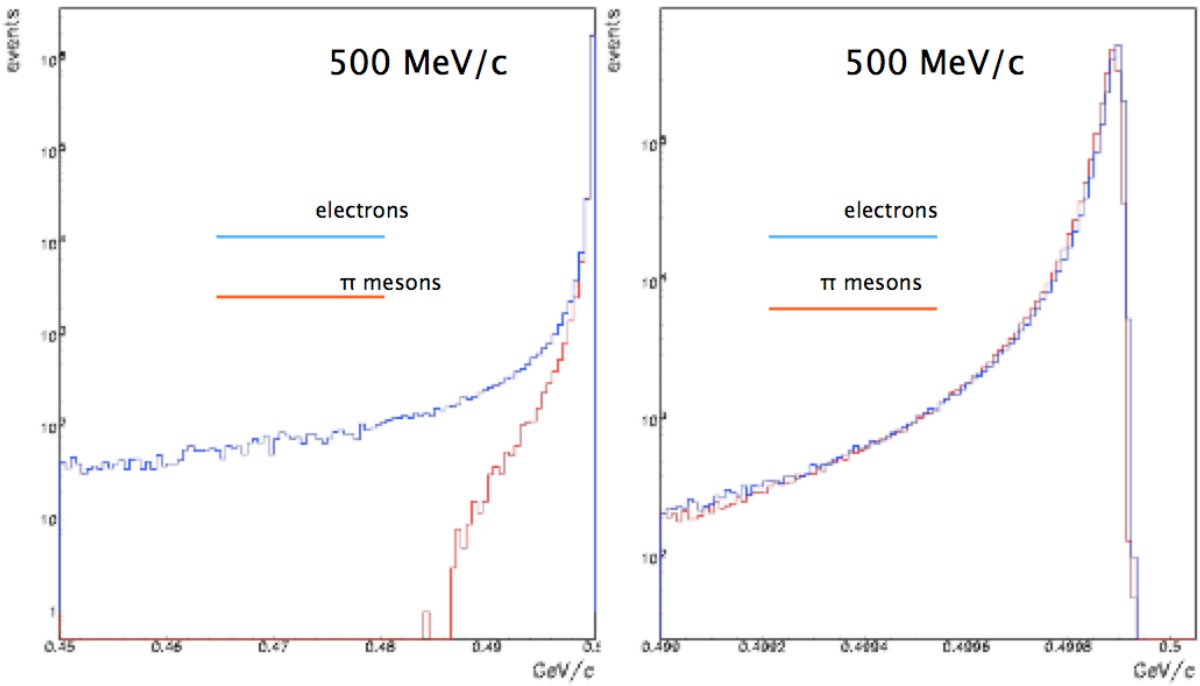

Fig.5. *Energy spectrum of a 500 MeV electron beam after passing 0.5 mm Be window.*

The recoil proton angle θ_R is given by the following expression:

$$\sin(\theta_R) = \frac{(\varepsilon_e + M)T_R}{P_e P_R} \tag{6}$$

Fig.6 shows dependence of θ_R and θ_e on the recoil proton energy T_R.

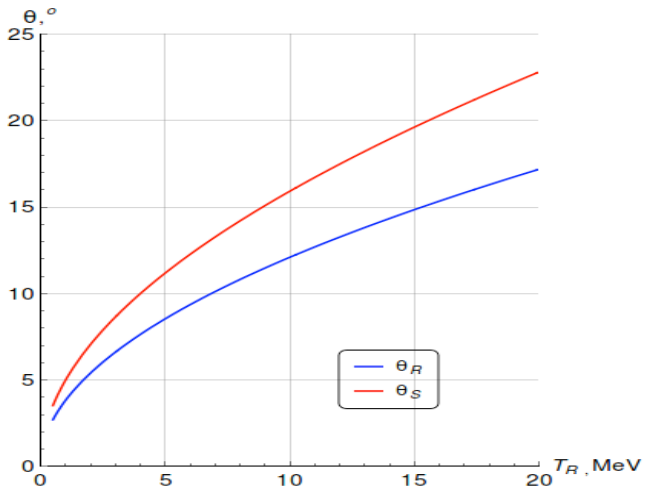

Fig.6. *Scattering electron and recoil proton angles as function of the recoil proton energy for 500 MeV electrons.*

The θ_e - T_R , θ_R - T_R , and θ_e - θ_R correlations can be used to eliminate the backgrounds. As an example, Fig.7 demonstrates the θ_e - T_R , θ_R - T_R, and θ_e - θ_R plots calculated for the ep elastic scattering and the background reaction $ep \rightarrow ep\pi^0$ for 900 MeV electrons. Note that θ_p in these plots corresponds to 90^o-θ_R. One can see that the elastic scattering can be well separated from the background.

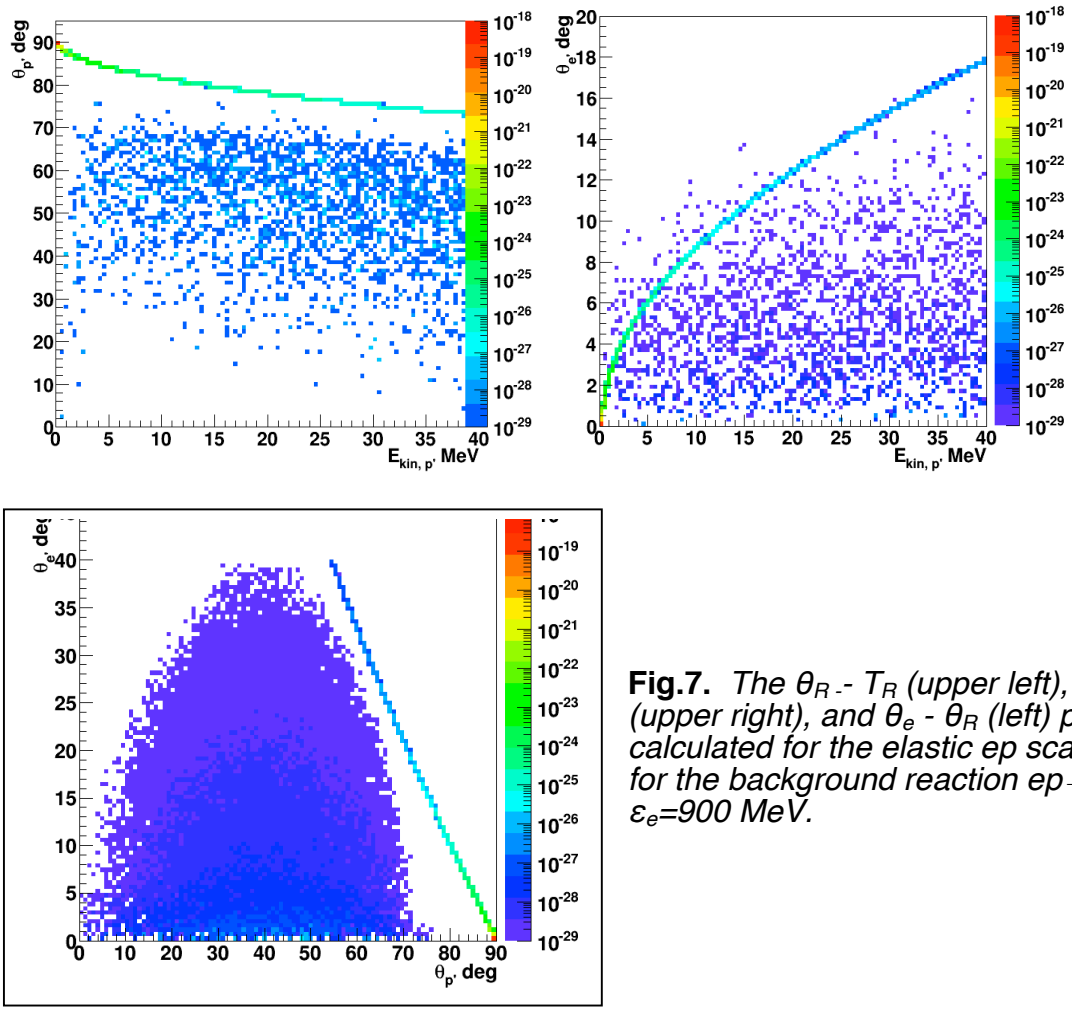

Fig.7. *The θ_R - T_R (upper left), θ_e - T_R (upper right), and θ_e - θ_R (left) plots calculated for the elastic ep scattering and for the background reaction $ep \rightarrow ep\pi^0$ at ε_e=900 MeV.*

An advantage of the proton recoil method is also relatively low radiative corrections, as the electron vertex correction and the corrections due to real photon radiation by electron cancel out each other almost exactly. On the other hand, the radiation from the proton side is suppressed by the large proton mass. So the analogous corrections coming from the proton side are much smaller (but must still be accounted for- this issue currently being under investigation).

3. Hydrogen Time Projection Chamber

The hydrogen TPC was developed at PNPI, and it has been used in various applications [2,3,4] including experiments WA9 and NA8 at CERN for studies of small angle πp and pp scattering at high energies. The experiment proposed here has much in common with WA9/NA8. But there are also essential differences. The absolute precision in $d\sigma/dt$ was 1% in WA9/NA8, while in the proposed experiment it should be 0.2%. To reach this goal, some innovations were implemented in the detector design and in the calibration procedures, in particular. In the proposed experiment, the high pressure hydrogen TPC and the large aperture Forward Tracker are placed in one vessel which could stand for pressures up to 25 bar (Figs.8 and 9). These detectors operate with different gas fillings: ultra-clean hydrogen in TPC and Ar+CH_4 in the tracker. The TPC volume is separated from the Ar filled space by the walls with a 0.1 mm Be window at the entrance and by a thin Mylar membrane in the downstream wall. The gas pressure in both volumes is permanently equalized. It is foreseen that two gas pressures will be used for the experiment: 20 bar and 4 bar, where the low pressure is used for finer resolution of the lowest Q^2 region.

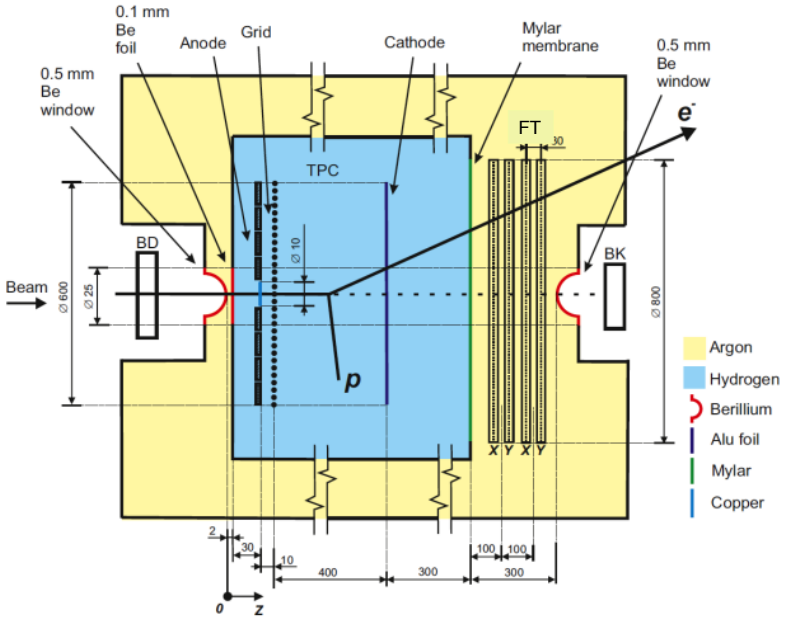

Fig. 8. *Schematic design of the TPC & FT detector.*

TPC geometry:
Cathode – Grid distance: **400.00 mm ± 40 μm;**
Anode – Grid distance: 10 mm.
Grid: 100 μm wires with 1mm spacing. Grid transparency ~1%.
TPC sensitive volume: 600 mm in diameter x 400mm.
The anode is subdivided into a central 10 mm in diameter circle and 7 rings (42 mm width each) (Fig.10).
Twenty field correction rings are placed in the outer TPC region between the cathode and the grid to form the uniform electric field in the drift space.
High Voltage:
-100 kV on the Cathode, -7 kV on the Grid, 0 kV on the anode at 20 bar pressure.
The HV is distributed for the field compensating rings with a resistor divider.

The HV will be known with **0.01%** absolute precision.

H_2 gas purity

In order to avoid the losses of the ionization electrons during the drift time, the contamination of the H_2 gas by any electro-negative gas (O_2, H_2O) should be reduced to a level below 1 ppm. This will be achieved by continuous H_2 purification with a special gas purification system,similar to that described in [5], which eliminates gas impurities down to **<0.1ppm.**

H_2 atomic density

The number of protons per cm^3, n, in hydrogen gas as a function of Pressure, P_{tech}, and temperature, t^0, is given by the following expression:

$$n = 5.2005 \cdot 10^{19} \cdot P_{tech} \cdot 273.16 \ / (1 + 0.000524\ P_{tech})\ (273.16 + t^0), \qquad (7)$$

where P_{tech} = 735.552 mmHg.

In our experiment, pressure will be controlled to **0.01%** absolute precision and temperature will be kept constant with **$\pm 0.05^0$** **(0.014%** absolute precision). This determines the proton density with **0.025%** absolute precision.

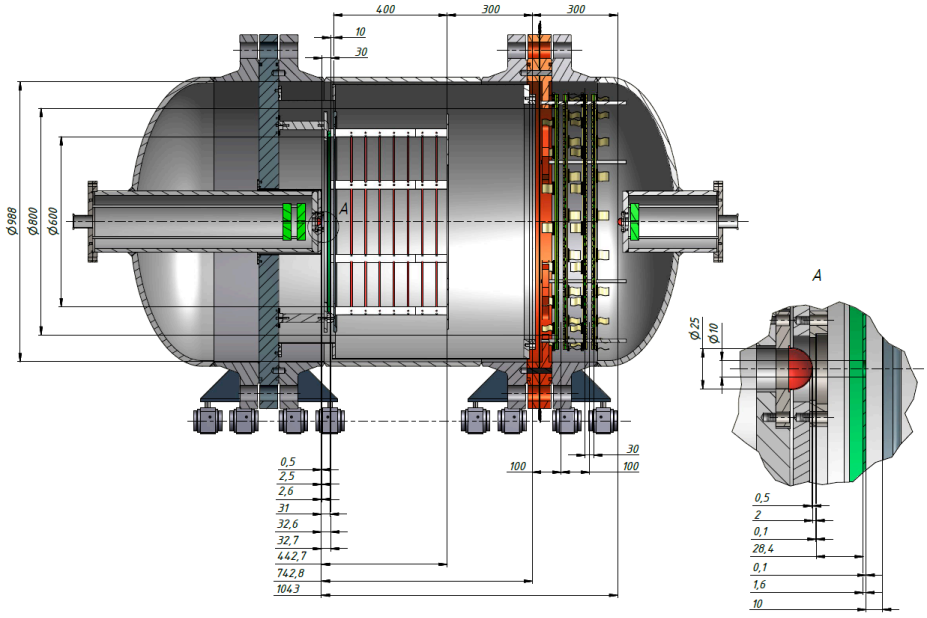

Fig.9. *Tentative design of the combined TPC & FT detector.*

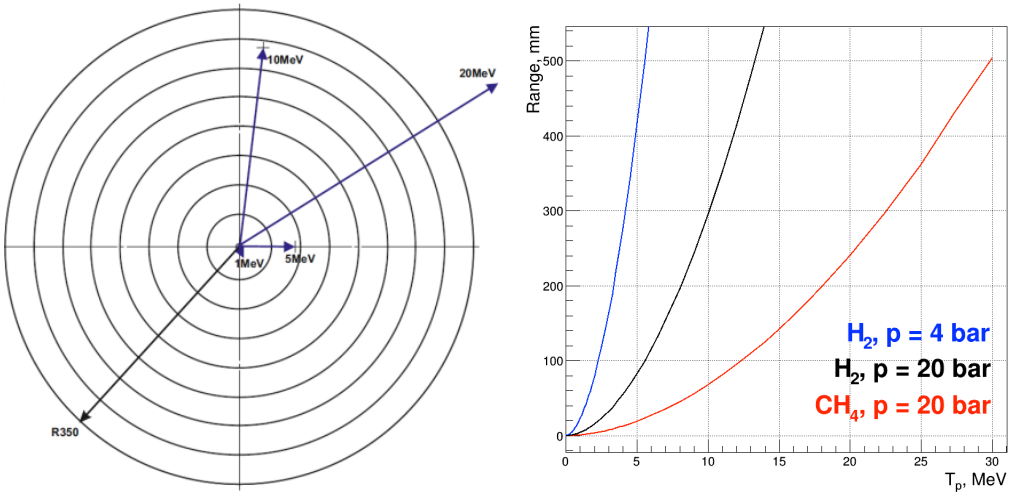

Fig. 10. *TPC anode structure: 10 mm in diameter circle surrounded by 7 rings (Left panel). Proton range-energy plots for H2 gas (20 bar and 4 bar) and for CH_4 (20 bar) (Right panel).*

Time, recoil energy, and recoil angle resolution :

The anode channels will be equipped with low noise preamplifiers with the noise at the level of **20 keV (sigma).** This determines the recoil energy resolution. Depending on the range of the recoil proton, the recoil energy is obtained by the sum of energies deposited against the anode rings. Accordingly, the noise will be summed up as well. So the energy resolution for maximal proton range (T_R~ 10 MeV for 20 bar, T_R~ 4 MeV for 4 bar) will be **around 60 keV (sigma)**. Note, however, that the noise might be larger in the presence of the electron beam. This should be checked in the test experiment with the electron beam.

The expected signal arrival time resolution is **40 ns (sigma).** The angular resolution in θ_R is limited by the Coulomb scattering of the recoiled protons: ~ **10 mrad (sigma).** θ_R is measured by the differences in arrival times of the signals from the anode rings crossed by the recoil (this is possible for tracks exceeding 60 mm, that is detected by at least two anode rings). The precison of such measurements varies from ~ ±10 mrad (signals from two neibour rings) to ~ ±2 mrad for long ranged protons.
So the final recoil angle resolution will be **from 15 mrad to 10 mrad** (for proton range 60-80 mm and ~ 300 mm, respectively).

Electron drift velocity and track diffusion in TPC

The electron drift velocity is $W_1 \approx 0.42$ cm/μs in the TPC drift region and $W_2 \approx 0.75$ cm/μs in the region anode-grid. The value of W_1 should be known with high precision (better than 0.1%) as it determines the selected gas target thickness (important for absolute dσ/dt measurements) and determines the Z-coordinate of the vertex used to measure θ_e.

The value of W_1 will be measured in special measurements by detecting time intervals between the beam trigger and the signals produced by the beam electrons crossing TPC perpendicular to the TPC axis at three Z- coordinates counted from the the HV plane: Z=10 mm, Z=200 mm, and Z=380 mm. Three Be windows in the TPC body will be arranged at these distances. The whole setup should be turned by 90 deg for these measurements (Fig.11). The distances between the selected Z- coordinates will be determined with 20 μm precision by precision shifting the setup across the beam direction. Note that the beam intensity should be reduced to 10^4 e/sec to exclude the overlapping signals in TPC. The expected precision in measurements of the drift velocity is **0.01%.**

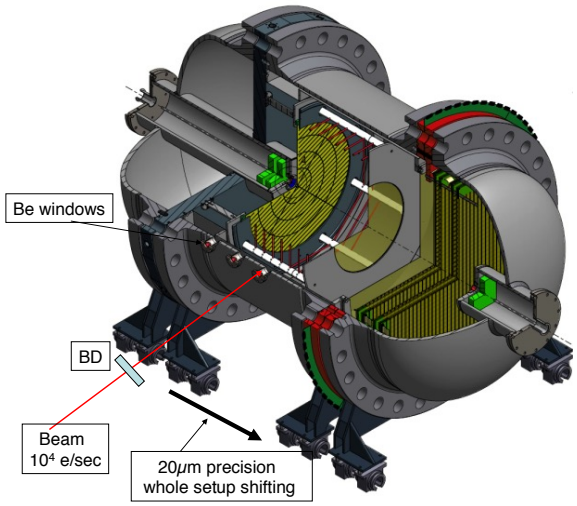

Fig.11. *Experimental layout for high precision measurement of electron drift velocity.*

The same measurements will provide information on track diffusion during the drift time by observation of the TPC signal width in function of the drift time. According to the available literature information [6], the track diffusion is rather small. In our experimental conditions it should be $\sigma_L \approx 0.006 \sqrt{L}$, that is **~ 400 μm (sigma)** for maximum drift distance L=40 cm. The diffusion is not important for measurements of W_1 where arrival time will be determined by the signal maximum. But it may have some effect on measurement of arrival times of the TPC signals which will be determined by the front-edge of the signals. In this case some small corrections to the measured arrival times may be needed. The magnitude of these corrections will be obtained in the diffusion measurements, mentioned above.

The drift velocity depends on the E/P (electric field / pressure) ratio in the drift space. The change in E/P by 1.5% changes W by 1%. In our experiment, both HV and the pressure will be kept stable and reproducible **on a level of 0.02%.** The W measurements will be performed at HV=100 kV, 95kV, and 90 kV. Similar measurements will be performed at 4 bar pressure with HV reduced by a factor of five.

Gas target length

The gas target length, L_{tag}, is determined from the measured difference between maximal and minimal arrival times of the TPC signals in the chosen drift space, $L_{tag} = (t_{arr\ max} - t_{arr\ min}) \cdot W_1$. Only a small correction to $t_{arr\ max}$ might be needed for track diffusion. The expected precision in L_{tag} determination is **0.02%** for L_{tag} =35 cm.

Vertex Z coordinate. Calibration and resolution.

The knowledge of the vertex absolute Z-coordinate is needed for measurement of the electron scattering angle. Calibration of the Z-scale will be done simultaneously with measurements of the drift velocity. The TPC setup will be slightly turned so that the electron beam (in position Z=10 mm) will cross the HV plane in the TPC central region thus producing ionization at Z close to Z=0. Registration of these signals can fix the Z scale in TPC with absolute precision **better than 100 μm**. Note that the electronics delays between the beam trigger and TPC signals should be identical to those in the main experiment.

Another way to determine Z = 0 can be detection of the signals produced by the beam electrons on the central anode in the nominal zero degree TPC position. The Z=0 point can be found by analyzing the end part of these ~ 100 μs long signals. Advantage: such measurements can be done at any time in the course of the main experiment (with beam intensity reduced to 10^3 e/sec). The main disadvantage is relatively large systematical uncertainty in determining the Z=0 point. The optimal solution would be calibration of this method by the 90 degree setup measurements. Then it can be used as a stability control for the Z scale calibration in the course of the experiment.

As to the Z resolution in detection of the recoil protons, it depends on the arrival time resolution. The Z-resolution is expected to be **σ_Z ~ 200 μm.**

4. Forward Tracker

The Forward Tracker is designed for high absolute precision in measuring the X and Y coordinates of the electron track relative to the beam line. Also, it provides fast signals for the trigger system. The FT consists of two pairs of Cathode Strip Chambers X_1/Y_1 and X_2/Y_2. Each chamber is a symmetric MWPC with 2.5 mm gap between the cathode and the anode planes. The size of the chamber is 600x600 mm^2. The readout is from both cathode planes. The anode wire plane will contain 30 μm wires spaced by 3mm. Both cathode planes will be made with 100μm (or 50 μm) wires wound with 0.5 mm step. The cathode wires are orthogonal to the anode wires in one cathode plane and parallel in the other cathode plane. The wires in the cathode plane with parallel cathode/anode wires are grouped into 10 mm strips. The fast signal from these strips will be used in the triggering system with ~5 ns resolution and for rough measurement of the coordinate of the track in direction perpendicular to the anode wires.

The key element of the CSC is the cathode plane with orthogonal cathode/anode wires. It determines the absolute measurements of the coordinate along the anode wire. In this plane, 2 mm strips will be formed by joining together 4 wires. The width of all

strips should be identical within ± 20 μm. This allows determination of the center-of gravity of each detected signal with a precision ~1% of the strip width (σ_{proj}~ 30 μm) assuming the signal to noise ratio S/N > 100 and the electronics amplification uniform within 1% in each readout channel. The most important requirement to the strip plane is that it should provide absolute linear scale with ~0.02% precision. We plan to reach this goal by developing high precision wiring and by final certification of the wire strip positions with a microscope.

To obtain the ratio S/N ≥ 100, the CSC gas gain should be ≥ $2 \cdot 10^4$. It is not trivial to obtain such gain at 20 bar pressure with 600 mm long anode wires. In particular, it is not possible in pure hydrogen. That is why we shall use Ar +CH_4 gas mixture. The CSC performance will be tested and optimized in a special CSC prototype.

There will be a dead zone in the centers of the CSCs (~ 20 mm in diameter) to reduce the sensitivity to the electron beam crossing the CSCs. This will be done by electrolytically depositing an additional gold layer on the anode wire in this spot. Note that some sensitivity still will remain, and it will be used in the CSC alignment procedure.

5. Beam detectors, Trigger, Acquisition

The beam detectors have several functions:

1) Measurement of each beam electron track at the TPC entrance. Upstream Pixel detectors, resolution **$\sigma_X = \sigma_Y = 30$ μm.**
2) Tracing the beam line. Up- and downstream Pixel detectors in coincidence. Precision: **$\sigma_X = \sigma_Y = 10$ μm** in the region of the FT detector.
3) Providing clean trigger signals Tr0 for acquisition. Two upstream detectors in coincidence. Time resolution ~ 10 ns.
4) Pileup rejection of the beam electrons in the trigger resolution time ~10 ns. A fast (100 ps) downstream scintillator detector (PILEUP detector).
5) Providing signals for non scattered electrons to be used as a beam killer in the off-line analysis. Downstream detector ~ 2 cm in diameter (Beam Killer).
6) Providing absolute counting of the incoming beam electrons for determination of the absolute cross sections. Precision: **0.05%**.

As an option, the beam detector system might consist of two upstream Si-pixel detectors and one downstream Si-pixel detector in combination with fast scintillation counters. The size of the pixel detectors might be ~ 3x3 mm^2.

The acquisition system will use continuous data flow. The coincidence of Tr0 with a fast signal from CSCs or anti-coincidence of Tr0 with the Beam Killer in ~ 10 ns time window will serve as a trigger Tr1 to save the data accumulated during the time interval 100 μs after Tr1 in all readout channels. The 12 bits 10 MHz and 12 bits 100 MHz ADCs will be used for digitization of the signals from TPC and FT, respectively.

The measured quantities are presented in Table 1. The efficiency in detection of the ep events triggered by Tr0 in the measured t-range should be close to 100%, the inefficiency being under control on a level of **0.05%**.

Table 1. The measured quantities and resolutions

	Measured quantity		Resolution,σ	comment
1	Recoil proton energy	T_R	40-60 keV	$T_R \leq 10$ MeV
2	Recoil proton angle	θ_R	15 -10 mrad	Recoil range > 60 mm
3	Z coordinate of ep vertex	Z_V	200 μm	
4	Time arrival of TPC signals	t_{arr}	40 ns	
5	X & Y coordinates in CSC	X/Y_{CSC}	30 μm	
6	Time arrival of CSC signals	t_{CSC}	5 ns	
7	X&Y coordinates in BD-1 *)	X/Y_{BD-1}	30 μm	
8	Time arrival in BD-1 signals	t_{BD-1}	10 ns	
9	X&Y coordinates in BD-2 *)	X/Y_{BD-2}	30 μm	
10	Time arrival in BD-2	t_{BD-2}	10 ns	
11	Time arrival in PILEUp detector	t_{PU}	0.1 ns	
12	Time arrival in Beam Killer	t_{BK}	1 ns	

*) BD-1 and BD-2 here stands for upstream and downstream detectors, respectively

6. Alignment

High precision alignment of various parts of the detector is needed for precision measurements of the electron scattering angle θ_e. Fig.9 presents a tentative design of the TPC@FT detector. In this design, the entrance flange is used as a reference plane in the alignment procedure:

* The TPC anode plane, grid plane, HV planes, and the plane of the block of CSCs will be set to be parallel to the entrance flange plane to **0.1 mrad precision**.
* Z distances between the TPC HV plane and the anode wire plane in each CSC as well as Z distance between the TPC HV plane and the TPC grid plane will be measured to **40 μm precision**.
* The whole detector should be installed in such a way that the entrance plane will strictly be **(± 0.1 mrad)** perpendicular to the beam line. This procedure is not fixed yet, to be discussed with MAMI experts.
* Only modest precision (± 1mm) in the X/Y alignment of CSCs is foreseen. The precise X=0, Y=0 position in CSCs will be measured by the beam tracing. The pixel detectors will determine the beam line while CSCs (in coincidence with Pixels) measure the X=0, Y=0 coordinates with **better than 20 μm precision.**

  The final control for the X=0, Y=0 position and for the angle between the detector planes and the beam axis will be done by the azimuthal symmetry analysis of the experimental data.

7. Azimuthal symmetry

In case of ideal alignments (that is when the electron beam is strictly perpendicular to the detector planes and crosses CSCs at X=0,Y=0), the azimuthal distributions of the detected events in the X-Y plane should be ideal circles at any θ_e. If the beam is displaced by ΔX (ΔY), this will shift the centers of the circles by $\Delta X(\Delta Y)$ relative to the initially chosen center (X=Y=0), independently on θ_e. On the other hand, the appearance of some angles ϕ_X (ϕ_Y) between the beam direction and the XZ (YZ) planes in CSCs will produce shifts proportional to $\phi_X \cdot z \cdot (tg\theta_X)^2$ and $\phi_Y \cdot z \cdot (tg\theta_Y)^2$, where z is the distance from of the ep vertex to the CSC anode plane. Fitting the experimental data with $\Delta X + \phi_X \cdot z(tg\theta_X)^2$ and $\Delta Y + \phi_Y \cdot z \cdot (tg\theta_Y)^2$, one could find ΔX, ΔY, ϕ_X , and ϕ_Y with estimated precision **± 20 μm** for $\Delta X(\Delta Y)$ and **± 0.1 mrad** for ϕ_X, and ϕ_Y. Note that the misalignments of this level has negligible effect on the measured θ_e distributions due to averaging over the whole azimuthal space.

8. Calibration of the t-scale

The critical point in the recoil proton method is extraction of the t-value from the observed TPC signal, S_{TPC}. One should take into account not only dependence of the produced ionization on the energy of the recoil proton but also several other factors: recombination, lost of electrons in the drift space (adhesion to O_2), grid transparency, shaping of the signal. Moreover, these effects depend on experimental conditions. The best way to solve this problem is to perform calibration of the TPC signals directly in the experimental setup.

The calibration of the TPC t-scale foreseen in this experiment relates the observed signals S_{TPC} with the absolute t-values determined from the measured θ_e distributions.

The calibration will be done using collected real experimental data. For that, in the 2D plot S_{TPC} - θ_e we select a bin ΔS_{TPC} and look at the corresponding θ_e distribution. This will be a peak at θ_{eM} with a tail to larger angles due to the energy losses of the electron before the ep collision. However, the maximum of the spectrum at θ_{eM} (with corrections for ionization losses in Be windows (Fig.5)) should correspond to the undisturbed incident beam energy ε_e thus allowing to determine the t-value corresponding to the selected S_{TPC} bin.

The main statistical error in determination of θ_{eM} comes from the electron multiple scattering. This leads to the θ_e dispersion ~1 mrad (sigma) at 500 MeV in the electron

detector region. However, the θ_{eM} position could be determined with 0.01mrad (sigma) around T_R =1MeV and with 0.02 mrad precision around T_R =10 MeV due to high statistics ($>10^5$ and $>10^4$ in each bin, correspondingly). Our θ_{eM} range goes from 85 mrad (T_R = 1MeV) to 270 mrad (T_R = 10 MeV) at 500 MeV**.** That means that the statistical error in θ_{eM} will be **on a level of 0.01%** in the whole T_R range.

To determine the absolute t-value, one should know the absolute values of θ_{eM} and ε_e. As to the absolute beam energy ε_e, it is known at MAMI with ± 120 keV at 720 MeV and with ± 140-160 keV at 570 MeV and at 855 MeV, respectively, that is with **~ 0.02%** precision. We can also mention the ongoing efforts at MAMI to further improve the accuracy of the absolute beam energy measurements.

The absolute precision in measurement of θ_{eM} is determined mostly by the linear scale in the CSC strip planes, and it is expected to be **0.02%** in the whole t-range from 0.002 to 0.04 GeV^2. Adding these two errors linearly, we can expect **0.08%** precision in absolute TPC t-scale calibration**.**

This procedure should be done for several intervals in the vertex Z positions to determine corrections for possible Z dependence of the TPC signals at fixed recoil proton energies.

Note that with the t-scale calibrated at one beam energy, one can use it at any other energy (also with other beam particles, gammas, for example) as the experimental setup guarantees reproducibility of all experimental conditions essential for the t-scale calibration (gas pressure, gas purity, temperature, high voltage, TPC readout...)

9. Statistics and beam time

The statistical error in the measured proton radius was estimated by simulating $1.7\cdot10^7$ ep scattering events in the t-range from 0.002 GeV^2 to 0.04 GeV^2. Such number of events could be collected during 30 days of continuous running with $2\cdot10^6$ e/sec beam with TPC operating at 20 bar with target thickness $3.6\cdot10^{22}$ protons/cm^2 (L_{target} = 35 cm). The results are presented in Fig. 12. The statistical error proved to be rather small: σ(Rp) =0.003 fm without normalization of the simulated data and σ(Rp) =0.002 fm with normalization factor set to 1. The real case with normalization error of 0.2% will be in between. In any case, these errors are smaller compared to our designed goal to measure the proton radius with σ(Rp) ≤ 0.006 fm.

Target thickness = $3.6\cdot10^{22}$ p/cm^2
P =20bar L =35cm
Beam intensity $2\cdot10^6$ sec^{-1}
Running time 30 days ($2.5\cdot10^6$ s)

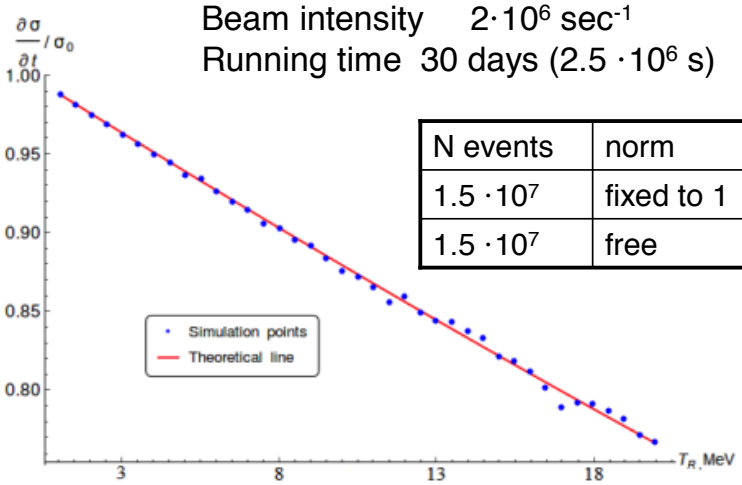

N events	norm	t-scale	σ(Rp)
$1.5\cdot10^7$	fixed to 1	fixed	± 0.002 fm
$1.5\cdot10^7$	free	fixed	± 0.003 fm

Fig. 12. *Simulation studies of statistical error in measurement of the proton radius.*

10. Systematical errors in relative and absolute measurements of dσ/dt.

The possible systematical errors were discussed in the text above. These errors are summarized in Table 2. Also shown how these errors contribute to the errors in dσ/dt.

One can see that the systematical errors are 0.1 % in the relative measurements of dσ/dt and 0.2% in the absolute measurements, which corresponds to the declared goal of this experiment.

Table 2. The systematical errors entering the measured dσ/dt

		Syst. Error %	comment
1	Drift velocity, W1	0.01	
2	High Voltage, HV	0.01	
3	Pressure, P	0.01	
4	Temperature, K	0.015	
5	H_2 density , ρ_p	0.025	Sum of errors 3 and 4
6	Target length, L_{tag}	0.02	
7	Number of protons in target, N_p	0.045	Sum of errors 5 and 6
8	Number of beam electrons, N_e	0.05	Clean Tr0 free of pileups
9	Detection efficiency	0.05	
10	Electron beam energy, ε_e	0.02	
11	Electron scattering angle, θ_e	0.02	
12	t-scale calibration, T_R relative	0.04	Follows from error 11
13	t-scale calibration, T_R absolute	0.08	Follows from the sum of errors 11 and 10
	dσ/dt , relative	0.1	0.08% from error 12
	dσ/dt , absolute	0.2	0.16% from err.13 plus errors 7,8, and 9

11. The layout of the experimental setup

The TPC&FT detector will be installed on the rails on a platform of 1.5m x 2.5m size (Fig.13). The detector can be moved along the rails for 400 mm under 20 μm precision control. The platform stands on three legs allowing smooth regulation in height. The legs have air pillows which allows tuning the detector position relative to the beam line.

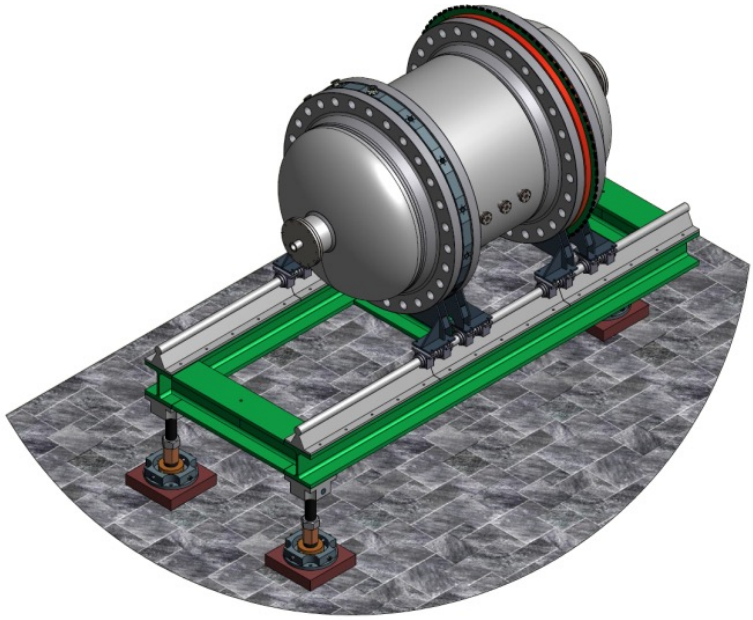

Fig. 13. *The TPC&FT detector on a movable platform.*

Fig. 14 shows a layout of the TPC&FT detector with corresponding infrastructure (the gas circulation/purification system, the high voltage system, the acquisition system etc.) All these systems will be placed into five racks. These racks could be installed in arbitrary place within 10 m distance from the TPC&FT detector. All communication lines from the racks to the detector will go via a vertical support allowing to turn the detector

by 90 degrees without dismounting the communication lines. The total area occupied by the TPC&FT detector is 3 x 3 meters. The body of the TPC&FT detector will be covered with a thermo-shirt with temperature stabilization $\pm 0.05^0$.

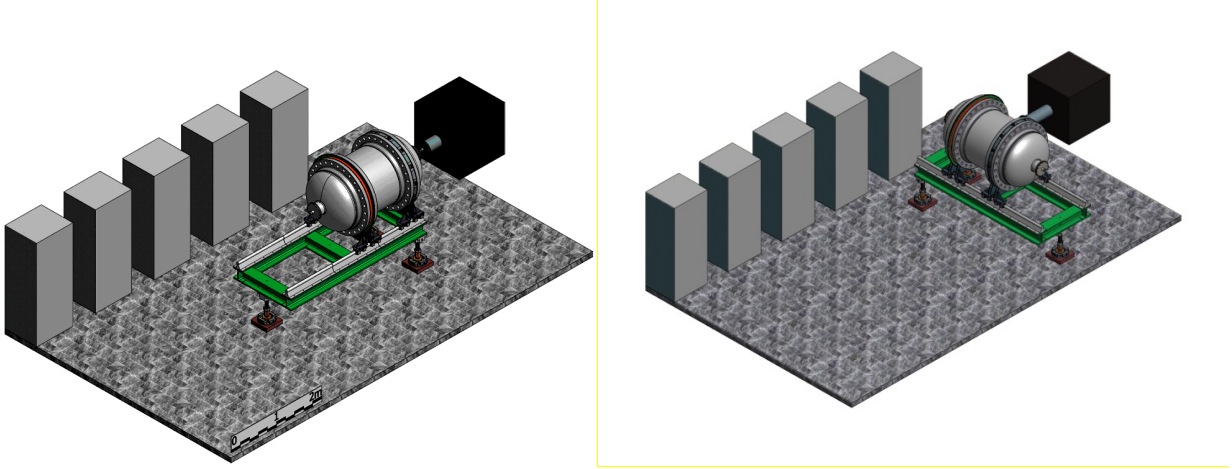

Fig.14. *Experimental layout for the physics run (left) and for drift velocity measurements (right).*

12. The working plan

In 2017, we plan to perform a test experiment with a 720 MeV electron beam at MAMI using an available experimental set up with a TPC prototype operating at 10 bar H_2 gas (section 13). This experiment has several goals:

- To study the background (noise in the TPC anode channels) created by the electron beam at $2 \cdot 10^6$ e/sec intensity. This will help to make final design of the TPC anode structure (decision on possible separation of the anode rings into azimuthal sectors).
- To measure the flux of created by the electron beam charged particles downstream of the TPC in the designed zone of the FT detector. This flux will determine the efficiency of the Tr1 trigger in the main experiment. Important for planning the acquisition system.
- To develop and to test the beam telescope system.
- To measure the parameters and to test the quality of the low intensity electron beam at $2 \cdot 10^6$ e/sec, at $\sim 10^4$ e/sec, and at $\sim 10^3$ e/sec.

We assume here that the A2 hall in principle can be operated with electrons (especially at such low currents). Further investigations are needed to be made, however, in order to be certain that the beam conditions are good enough for such an experiment.

The first physics run is planned for the second half of 2018 in the 720 MeV electron beam. This run will be started with drift velocity measurements as described in section 2. The experimental setup will be in position 90 degree with respect to the beam line (section 11). These measurements require a 10^4 e/sec intensity beam with divergency ≤ 0.5 mrad. The measurements will be performed at 20 bar and at 4 bar H_2 pressure at several HV values. This will require three days of the beam time.

The physics run will be performed with the same electron beam but in the setup position Zero degree with respect to the beam line (section 11). The first task will be to install the TPC&FT detector along the beam line with 0.1 mrad precision and to control this alignment with TPC and FT signals produced by the beam electrons. This requires a very low intensity beam $\sim 10^3$ e^-/sec. This procedure might need 3 running days. After that - the main run with $2 \cdot 10^6$ e^-/sec beam. Two weeks at 20 bar pressure and 1 week at 4 bar pressure. The goals of this experiment are to perform the t-scale calibration, as described in section 7, and to obtain the first results in measurements of the proton radius.

One of the reasons to choose the beam energy 720 MeV is that it is known with the best absolute precision $\delta\varepsilon_e/\varepsilon_e = 1.7 \cdot 10^{-4}$ which is important for the t-scale calibration.

The experimental setup guarantees reproducibility of all experimental conditions essential for the t-scale calibration and for the drift velocity measurements (gas pressure, gas purity, temperature, high voltage, TPC readout, etc). Therefore, the t-scale and drift velocity should not be remeasured in each new run and with changing the beam energy.
The plan is to perform high statistics studies at 720 MeV and at ~ 500 MeV at 20 bar and also at 4 bar pressure for better control of the low t-region.

13. Experimental set up for a test experiment in 2017

In the 2017 test experiment at MAMI we plan to use the available experimental setup which was constructed within the program FAIR at GSI as an ACTAR2 prototype of the Active Target for the R3B experiment. In April 2014, the prototype has been used in a test experiment at GSI with 700 MeV/u heavy ions beams. This prototype is a TPC similar to the TPC in our proposal (only smaller in size and with lower pressure), and it can help to solve the tasks formulated in section 12.

A schematic view of the layout of the ACTAR2 prototype is shown in Fig. 15. The system of the TPC electrodes – the cathode, the grid and the sectioned plane of anodes is placed inside a 40 liters cylindrical aluminum vessel of 600 mm length with the internal diameter of 288 mm, the wall thickness being 4 mm. The semi-spherical beam windows of beryllium, 0.5 mm thick, 70 mm in diameter are mounted on the forward and backward flanges of the vessel.

The anode-grid distance is 3 mm, the grid-cathode distance (the drift gap) is 220 mm. The field uniformity in the drift gap is improved by a set of 11 copper rings (field shaping rings, see Fig. 15) placed around the sensitive volume with 18 mm step (rings of 230 mm diameter, 1 mm gauge). The grid is made of a stainless steel ring (of 204 mm internal diameter) with 55 μm in diameter steel wires wound with 1 mm step. The anode electrode is split into 66 segments (Fig. 16). The cathode and the grid of the TPC will be under –24 kV and –1.2 kV, respectively. The H_2 gas pressure will be 10 bar.

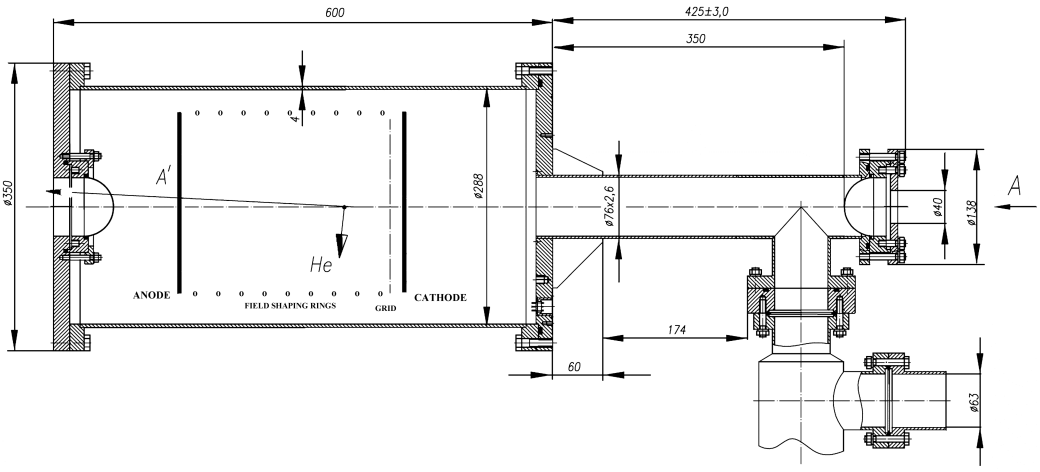

Fig. 15. *Schematic view of the ACTAR2 prototype (side view).*

Signals from all anodes are read out by independent electronics channels including preamplifiers, amplifiers, and Flash-ADCs (14 bit, 250 MHz). The energy resolution in each anode channel is $\sigma(T_R) \approx 20$ keV. The beam tracking detectors will be placed upstream and downstream of the ACTAR2 prototype. The general start of the readout system is triggered by the beam detectors. The information from all FADCs is recorded if a sufficiently large pulse is present at least at one of the segmented anodes.

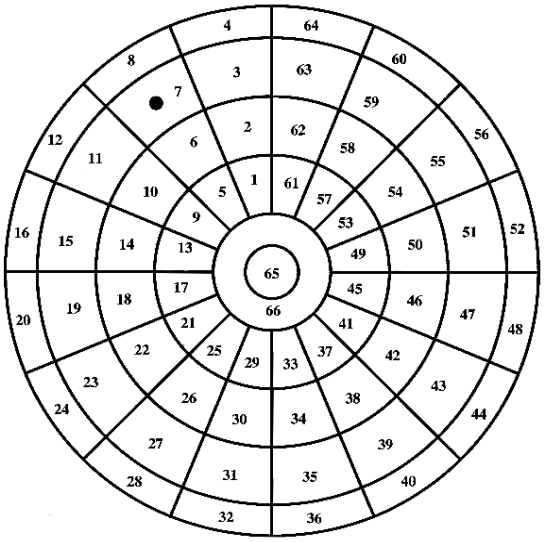

Fig. 16. *Layout of the ACTAR2 prototype anodes. An ^{241}Am α-source is deposited on the cathode of the chamber opposite to the black spot on the anode number 7. The outer diameter of the anodes is 200 mm.*

14 . Beam requirements

MAMI Specifications

Beam energy	500 MeV, 720 MeV
Energy spread	< 20 keV (1σ)
Energy shift	< 20 keV (1σ)
Absolute energy	±< 150 keV (1 σ)

Electron Beam Specifications

Beam intensity (main run)	2x10^6 e^-/sec
Beam intensity for calibration	10^4 e^-/sec and 10^3 e^-/sec
Beam divergency	≤ 0.5 mrad
Beam size	minimal at given divergence

Beam Time Request

Test run in 2017	~ 2 weeks
First physics run in 2018	~ one month

References:

1. Conference at Trento, June 2016. http://www.ectstar.eu/node/1659.

2. Soft πp and pp scattering in the energy range 30 to 345 GeV. Experiments WA9/NA8 at CERN.
   J.P. Burq *et al*. Nucl. Phys.B 217 (1983) 285-335.

3. Study of nuclear matter distribution in neutron-rich Li isotopes. Experiments at GSI.
   A.V. Dobrovolsky *et al*. Nucl.Phys.A 766 (2006) 1-24.

4. Precision measurement of the rate of muon capture in hydrogen gas and determination of the proton pseudoscalar coupling. Experiment MuCap at PSI.
   V.A. Andreev et al. Phys.Rev.Lett. 110, 022504 (2013).

5. A circulating hydrogen ultra-high purification system for the MuCap experiment.
   V.A. Andreev *et al*. NIM A578 (2007) 485.

6. Theory of Electron Diffusion Parallel to Electric Fields. II. Application to Real Gases.
   J.J. Lowke and J.H. Parker Phy.Rev. v181 № 1 (5 May 1969).